NASA Technical Paper 1598

Effects of a Ceramic Coating on Metal Temperatures of an Air-Cooled Turbine Vane

Herbert J. Gladden and Curt H. Liebert

FEBRUARY 1980

NASA

NASA Technical Paper 1598

Effects of a Ceramic Coating on Metal Temperatures of an Air-Cooled Turbine Vane

Herbert J. Gladden and Curt H. Liebert
Lewis Research Center
Cleveland, Ohio

National Aeronautics
and Space Administration

**Scientific and Technical
Information Office**

1980

SUMMARY

An experimental study was made to determine the effects on metal temperatures of using the NASA thermal-barrier coating system on an air-cooled turbine vane and to quantify the beneficial effects of this coating compared with the same vane without the ceramic coating. Effects of simulated coating loss, at the leading- and trailing-edge regions, were also investigated. These tests were made in a four-vane cascade over a range of inlet gas Reynolds numbers simulating current and advanced gas-turbine engines. The results of this investigation revealed that the ceramic coating generally reduced the airfoil metal temperatures, both locally and on the average, in proportion to the coating thickness. However, at low gas Reynolds number, where an apparent laminar boundary layer developed on the uncoated-vane suction surface, the ceramic coating tripped the boundary layer and resulted in higher metal temperatures because of the higher heat flux.

Coating loss was simulated by artificially removing segments of the ceramic coating in the leading- and trailing-edge regions of the vane. The effect was to sharply increase the local metal temperature at the point of the coating loss. However, the metal-temperature level in the leading-edge region remained below that of the uncoated vane. The trailing-edge temperature increased to a level higher than that of the uncoated vane primarily because a laminar boundary layer was tripped to the turbulent state by the coating for the gas conditions investigated.

INTRODUCTION

Cycle and mission studies of gas-turbine engines for advanced commercial and military aircraft show that turbine inlet temperatures as high as 1900 K (2960° F) with pressure ratios to 40 are used to provide the desired performance. Efficient cooling schemes are required for the hot-section components of these engines in order to maintain metal temperatures and temperature gradients at acceptable levels.

Two cooling schemes that may satisfy the cooling requirements in a high-temperature and -pressure environment, when combined with effective convection cooling, are the thermal-barrier coating (ref. 1) and full-coverage film cooling (refs. 2 and 3). The full-coverage film cooling concept has been discussed extensively in the literature and has been shown capable of reducing average airfoil metal temperatures to acceptable levels. Reference 2 discusses the potential benefits of combining an effective convection cooling scheme with full-coverage film cooling and indicates that substantial benefits

can be derived. However, temperature gradients and stress concentrations around the film cooling holes, which can have a detrimental effect on component life, occur with this concept. In addition, these types of film cooling configurations are expensive to produce and generally have higher aerodynamic losses (ref. 3) than entire convection-cooled airfoils.

Preliminary tests of a thermal-barrier coating system on turbine vanes and blades showed that it also has the potential of reducing metal temperatures to acceptable levels (refs. 4 to 7). These tests, however, concerned primarily the durability of the coating system. The overall effect of the coating on local and average metal temperatures, the effect of thermal gradients, and the effect of coating loss on local metal temperatures have not been studied. An experimental investigation was therefore made of these heat-transfer characteristics on a ceramic-coated, air-cooled turbine vane and on the same vane without a coating.

These steady-state heat-transfer tests were conducted in a four-vane, hot-gas cascade facility. Metal temperatures were measured around the airfoil periphery of the test vane with and without a ceramic coating. Coating thicknesses of 0.025 and 0.050 centimeter (0.01 and 0.02 in.) were investigated. The effects of coating loss at the leading- and trailing-edge regions of the vane were also simulated by artificially removing a segment of the coating in the desired area of the vane midspan.

The experimental data were taken over a range of gas-side Reynolds numbers of 0.28×10^5 to 1.65×10^5, which are based on turbine inlet free-stream conditions and the turbine vane leading-edge diameter. Gas total temperatures and pressures investigated were 590 to 1530 K (600° to 2300° F) and 22 to 86 N/cm^2 (32 to 125 psia). Ratios of coolant flow to gas flow investigated were 0.014 to 0.062. These tests were made at reduced conditions simulating current and advanced gas-turbine engines at takeoff and cruise conditions. The data are presented as plots of dimensionless metal wall temperatures against vane periphery for a variety of the test conditions for coated and uncoated vanes.

SYMBOLS

C_p	specific heat at constant pressure
D	leading-edge diameter
h	heat-transfer coefficient
k	thermal conductivity
L	surface distance (leading- to trailing-edge stagnation point)
L_1^*, L_2^*, L_3^*	dimensionless geometric terms

ℓ	characteristic dimension in Nusselt number
Nu	Nusselt number, $h\ell/k$
P	pressure
Pr	Prandtl number, $C_p\mu/k$
R	gas constant
Re	Reynolds number, $\rho vD/\mu$
T	temperature
T*	dimensionless wall temperature, $(T_w - T_c)/(T_g - T_c)$
V	velocity
w	mass flow rate
x	surface distance from leading-edge stagnation point
Γ	function of γ as defined by eq. (2)
γ	specific-heat ratio
μ	viscosity
ρ	density
τ	wall or coating thickness
φ	cooling effectiveness, $(T_g - T_w)/(T_g - T_c)$

Subscripts:

c	coolant
e	engine conditions
g	gas
i	inlet
TBC	thermal-barrier coating
t	test conditions
uc	uncoated
w	wall

Superscript:

$(\bar{\ })$	average

APPARATUS AND TEST PROCEDURE

Cascade Facility

The cascade facility was designed for continuous operation at gas temperatures and pressures to 1600 K (2420° F) and 100 N/cm^2 absolute (145 psia). A schematic cross-sectional view of the cascade facility is shown in figure 1(a). The facility consisted of five components: an inlet section, a combustor section, a circular-to-annular transition section, the test section, and an exit section. The transition, test, and exit sections were water cooled to achieve structural durability during high-temperature operation. A more detailed description is contained in reference 8.

The combustor section was removed and replaced by a spool piece for low-temperature tests in the facility. Hot combustion air was then supplied to the test section by the auxiliary combustor system shown in figure 1(b). The combustor in the auxiliary system was capable of supplying combustion air to the test section at temperatures to 900 K (1200° F).

The test section was a 23° annular sector of a vane row and contained four vanes and five flow channels. A plan view of the test section showing the central two test vanes, the outer slave vanes, and selected instrumentation is presented in figure 2. The outer slave vanes complete the flow channels for the test vanes and also serve as radiation shields between the test vanes and the water-cooled walls of the test section. The test-section walls were coated with yttria-stabilized zirconia in order to increase its surface temperature and thus to minimize the net radiation loss from the vane.

The cooling air was supplied to the two test vanes from a common manifold and the flow rate was measured by a venturi flowmeter. The cooling air to each of the outer slave vanes was supplied from separate cooling-air systems.

Three view ports in the test section were positioned so that portions of the test vane surface could be observed with optical temperature-measuring devices (fig. 2). Each view port contained a 1.3-centimeter- (0.5-in.-) thick quartz disk for viewing purposes. View ports 1 and 2 permitted observation of the leading-edge pressure and suction surfaces, respectively, of the two test vanes. View port 3 permitted observation of the trailing-edge suction surface of the test vanes. The dashed lines in figure 2 indicate the approximate chordwise surface area that could be observed from the view ports. The lines of sight from the three view ports were in a horizontal plane that passed through the midspan region of the test vanes.

Vane

The turbine vane used in this investigation was a J-75-size airfoil with impingement cooling in the forward two-thirds of the airfoil and combined pin-fin and film cooling in the aft one-third of the airfoil. A cross-sectional schematic of the airfoil and cooling configuration is shown in figure 3(a). A static- to inlet total-pressure ratio distribution for this type of airfoil in this facility (ref. 9) is shown in figure 3(b). The vane span was 9.78 centimeters (3.85 in.) and the midspan chord length was 6.28 centimeters (2.47 in.). The wall thickness in the impingement-cooled region was 0.152 centimeter (0.06 in.). The vane airfoil shell material was MAR M-302.

The impingement insert had a staggered array of holes that were 0.051 centimeter (0.02 in.) in diameter. The spacing varied, depending on location, between 6.5 and 9 hole diameters spanwise and between 2.4 and 9 hole diameters chordwise. The closely spaced holes were in the leading-edge region (6.5 by 2.4); the midchord region had larger spacings (9 by 9 on the pressure side and 8.5 by 8.5 on the suction side). The spacing between the impingement holes and the heat-transfer surface was approximately 1.5 hole diameters in the midchord region and approximately 2 hole diameters in the leading-edge region. The impingement insert material was L-605.

There were seven chordwise rows of round pin fins in the split trailing edge. The three upstream rows had pin diameters of approximately 0.102 centimeter (0.04 in.) with a spanwise spacing of 0.406 centimeter (0.16 in.) and a chordwise spacing of 0.353 centimeter (0.14 in.). The last four rows had pin diameters of 0.076 centimeter (0.03 in.) with a spanwise spacing of 0.305 centimeter (0.12 in.) and a chordwise spacing of 0.264 centimeter (0.104 in.). The width of the split-trailing-edge channel at the point of discharge was 0.089 centimeter (0.035 in.).

A single row of film cooling holes located between pin-fin rows 3 and 4 on the vane pressure surface ejected air at an angle of 30° to the vane surface in the spanwise direction. The purpose of these holes was to provide a sufficient flow area to accommodate the design coolant flow requirements.

Thermal-Barrier Coating

The procedure used for depositing the ceramic coating (ref. 6) onto the vane metal substrate was to prepare the substrate surface by grit blasting, to plasma spray on a bond coat of NiCrAlY, and then to plasma spray on the ceramic coating of yttria-stabilized zirconia. The measured surface roughness of the applied ceramic coating was 8 to 10 micrometers rms (315 to 395 μin.). However, the coating surface was polished with silicon carbide paper to a surface finish of about 3 micrometers rms (120 μin.).

The bond and ceramic coatings were built up to the desired thickness by a succession of spray applications in the spanwise and chordwise directions on the airfoil. The coatings were first applied to the vane leading edge, then to the trailing edge, and finally to the suction and pressure surfaces. The total coating thickness was determined, after the polishing operation, by comparing 10X profiles of the airfoil before and after coating at each of the thermocouple locations. The ceramic coating thickness was then assumed to be the total thickness less the approximately 0.010-centimeter- (0.004-in.-) thick bond coat. The ceramic coating was applied and tested at two thicknesses. The distribution of the coating thickness is given in table I. In each case, the coating was tapered to negligible thickness at thermocouple location 12 (fig. 3(a)). This was necessary because of the film cooling holes aft of this location. The coating techniques were not sufficiently developed at the time to permit coating in the hole region without hole blockage.

Coating spallation was simulated by removing the coating in selected spots. The coating was removed in a circular or elliptical pattern by masking the surrounding area and grit blasting the exposed surface until the coating was eroded down to the bond coat, as shown in figure 4. The vane locations selected for coating removal were thermocouple locations 1 and 6 (fig. 3(a)) on vane 2 and thermocouple location 8 on vane 3. Location 1 was about 1.0 centimeter (0.4 in.) in diameter; locations 6 and 8 were about 1.0-centimeter by 0.65-centimeter (0.4-in. by 0.25-in.) ellipses.

Test Procedure

The test conditions are given in table II. The desired combustion-gas temperature, pressure, and exit critical velocity ratio (0.85) were established and then the cooling-air flow rate was varied in a stepwise fashion from test point to test point. Steady-state data were recorded at each cooling-air and gas-condition point. Each gas condition listed in table II was repeated for tests of the uncoated vane and for tests of the vane with two ceramic coating thicknesses. The tests with simulated coating loss were terminated after testing at one gas condition because a coating crack had developed on vane 3.

The gas conditions used represent current and advanced gas-turbine engines such as a supersonic transport (SST) engine, a short-takeoff-and-landing (STOL) engine, a conventional-takeoff-and-landing (CTOL) engine, and a vertical-takeoff-and-landing (VTOL) engine. These gas conditions are also presented in terms of inlet gas Reynolds numbers based on the vane leading-edge diameter.

INSTRUMENTATION

The instrumentation used for the tests can be separated into two categories: the general operational instrumentation, and the research instrumentation. The operational instrumentation was used to establish gas and coolant conditions and to monitor the general conditions of the cascade and its supporting systems. Most of this instrumentation and various computed parameters were monitored continuously in the control room. The research instrumentation was concentrated on or around the test vanes within the central flow channel and was designed to provide data for detailed analysis of the cooling performance of the test vanes. The research data were recorded by a central data-recording system.

The research instrumentation provided detailed information on the gas-stream conditions, the cooling-air flow conditions, and the vane wall-temperature distribution. A radially traversing, sonic-aspirated, type R (Pt/Pt-13Rh) total-temperature probe and a radially traversing total-pressure probe were located upstream of the vane row (fig. 2). The temperature distribution was measured upstream of channel 3, and the pressure distribution was measured upstream of channel 4. The inlet static pressure was measured only at the inner radius (hub) and was assumed to be constant across the gas stream. Static pressures were also measured at the exit midchannel position of channels 2, 3, and 4 at both the inner and outer (tip) radius platforms. These pressures were used to establish the midspan inlet and exit critical velocity ratios.

The midspan of each test-vane airfoil was instrumented with an array of 12 Chromel-Alumel thermocouples. Figure 3 shows the relative location of these thermocouples with respect to the important features of the vane. Chordwise thermocouple locations are given in table I. The thermocouples were installed in slots electrical-discharge machined in the exterior surface of the airfoil. The junction end of each thermocouple assembly was peened into the slot, and thus the measuring station was effectively located a specified distance from the bottom of the slot. The remainder of the slot over the thermocouple junction was filled by spot welding a nickel-chromium material in the void and fairing the resultant construction to the original airfoil profile.

The thermocouple assemblies were constructed of Chromel-Alumel thermoelements with magnesium oxide insulation in an Inconel-600 sheath. These assemblies were drawn to two sheath sizes (0.050 and 0.025 cm (0.02 and 0.01 in.) outside diameter) with a closed-end, grounded junction formed at one end. The three thermocouples nearest the leading edge were 0.025 centimeter (0.01 in.) in diameter; the remaining thermocouples were 0.050 centimeter (0.02 in.) in diameter. The procedures for thermocouple construction are described in detail in reference 10. The slots for the 0.050-centimeter- (0.02-in.-) diameter thermocouples were 0.06 centimeter (0.024 in.) square; the slots for the 0.025-centimeter- (0.01-in.-) diameter thermocouples were

0.03 centimeter (0.012 in.) square. The measuring stations were nominally located 0.047 and 0.022 centimeter (0.019 and 0.009 in.), respectively, below the gas-side surface of the airfoil.

ANALYSIS METHODS

Similarity

The test data presented herein are related to actual engine performance data by the similarity constraints discussed in references 11 to 13. Similarity permits turbine vanes to be tested and evaluated in a less severe environment than that which exists in an actual gas-turbine engine. Reference 11 uses differential similarity to establish many dimensionless terms that must be equated between engine and test conditions in order to assure that test results can be used to represent the turbine-vane aerodynamic and thermal performance in an engine. The conclusions of reference 11 also verify the physical insight approach used by references 12 and 13. The references conclude that aerodynamic similarity can be approximated by maintaining an equality of Reynolds number, momentum thickness, and the critical-Mach-number distribution. This allows the test and engine conditions to be expressed in a functional relation of temperature and pressure:

$$\left(\frac{P_g}{\mu_g}\frac{\Gamma_g}{\sqrt{RT_g}}\right)_t = \left(\frac{P_g}{\mu_g}\frac{\Gamma_g}{\sqrt{RT_g}}\right)_e \tag{1}$$

where

$$\Gamma = \sqrt{\gamma}\left(\frac{2}{\gamma+1}\right)^{(\gamma+1)/[2(\gamma-1)]} \tag{2}$$

Figure 5 displays this relation for various current and advanced turbofan engines and the test conditions of this report. Each circular symbol on the figure represents an engine condition; the diamond symbol on the same curve represents the equivalent (similarity) test condition. The test and engine conditions investigated, as obtained from reference 13, are specified in table II. The gas Reynolds number in the table is used as a reference and is based on the gas inlet free-stream velocity and the vane leading-edge diameter, $Re = \rho VD/\mu$.

Similarity of coolant conditions between engine and test requires an equality of coolant Reynolds number, coolant- to gas-flow ratio w_c/w_g, and coolant- to gas-viscosity ratio, μ_c/μ_g. The gas- to coolant-temperature ratio, which is required for similarity of the gas- to coolant-momentum ratio, is also nearly duplicated by this method.

Reference 11 shows that the similarity of the test and engine Nusselt numbers is maintained if a similarity of temperature and velocity fields and Prandtl number is maintained between test and engine conditions. A functional relation of the significant heat-transfer terms can be developed through a one-dimensional heat balance. Radiation heat-transfer effects are neglected. For an uncoated turbine vane,

$$\left(\frac{T_g - T_w}{T_g - T_c}\right)_{uc} = \left[1 + \frac{(Nu)_g}{(Nu)_c} L_1^* \frac{k_g}{k_c} + (Nu)_g L_2^* \frac{k_g}{k_w}\right]^{-1} \tag{3}$$

For a ceramic-coated turbine vane,

$$\left(\frac{T_g - T_w}{T_g - T_c}\right)_{TBC} = \left[\frac{1 + (Nu)_g L_3^* \frac{k_g}{k_{TBC}}}{1 + \frac{(Nu)_g}{(Nu)_c} L_1^* \frac{k_g}{k_c} + (Nu)_g L_2^* \frac{k_g}{k_w} + (Nu)_g L_3^* \frac{k_g}{k_{TBC}}}\right] \tag{4}$$

The wall temperature T_w is assumed to be the gas-side surface temperature for the uncoated vane and the metal-ceramic interface temperature for the ceramic-coated vane. The temperature difference ratio on the left of equations (3) and (4) is commonly called the vane cooling effectiveness φ and is the same for both the test and engine conditions, provided the similarity constraints are satisfied. Experimental data are used to define φ where the inlet total gas temperature T_g and the inlet total coolant temperature T_c are substituted for local values. Geometry similarity is assued by using prototype-engine hardware for the tests. The dimensionless geometry terms L_1^*, L_2^*, and L_3^* are ratios of the characteristic dimensions in the gas and coolant Nusselt numbers, the metal wall thickness, and the ceramic coating thickness.

Thermal Conductivity Correction

Additional terms and ratios that must be considered for true similarity of test conditions are discussed in reference 11. However, for most tests, these additional terms

are neglected. This approach is acceptable if the test data are insensitive to the terms neglected. Reference 14 shows that material thermal conductivity can have a particularly significant effect on the results when comparing ceramic-coated- and uncoated-vane temperature data. Since the prototype-engine hardware is generally used in the tests, material thermal conductivity corrections are required.

Examination of equations (3) and (4) shows that the material thermal conductivities are contained explicitly in ratio form (k_g/k_w and k_g/k_{TBC}). The gas- to coolant-thermal-conductivity-ratio k_g/k_c similarity is satisfied by previous considerations. Reference 14 further shows that the cooling effectiveness parameter φ can be corrected for differences in these ratios between engine and test conditions.

$$\varphi_e = \varphi_t + \Delta\varphi_{e-t} \tag{5}$$

This correction factor for the uncoated vane is

$$\Delta\varphi_{e-t,\,uc} = -\varphi^2_{t,\,uc}\left(\frac{h_g \tau_w}{k_g}\right)_t \Delta\left(\frac{k_g}{k_w}\right)_{e-t} \tag{6}$$

where

$$\Delta\left(\frac{k_g}{k_w}\right)_{e-t} = \left(\frac{k_g}{k_w}\right)_e - \left(\frac{k_g}{k_w}\right)_t$$

The correction factor for the ceramic-coated vane is

$$\Delta\varphi_{e-t,\,TBC} = \varphi^2_{t,\,TBC}\left[\frac{\left(\frac{1-\varphi}{\varphi}\right)_{t,\,TBC}\left(\frac{h_g \tau_{TBC}}{k_g}\right)_t \Delta\left(\frac{k_g}{k_{TBC}}\right)_{e-t} - \left(\frac{h_g \tau_w}{k_g}\right)_t \Delta\left(\frac{k_g}{k_w}\right)_{e-t}}{\left(1 + \frac{h_g \tau_{TBC}}{k_{TBC}}\right)_t}\right] \tag{7}$$

where

$$\Delta\left(\frac{k_g}{k_{TBC}}\right)_{e-t} = \left(\frac{k_g}{k_{TBC}}\right)_e - \left(\frac{k_g}{k_{TBC}}\right)_t$$

Thermodynamic and transport properties are taken from reference 15. The thermal conductivity of the vane material and the ceramic are taken from references 16 and 17, respectively. For the purposes of this report, the gas-side heat-transfer coefficient is assumed to be an average value for the vane based on the turbulent flat-plate correlation.

$$h_g = 0.0296\left(\frac{k_g}{L}\right)Re^{0.8}\ Pr^{0.33} \tag{8}$$

Dimensionless Temperature Difference

In some cases, it is more convenient to show the results of the test as a dimensionless wall temperature rather than as a cooling effectiveness.

$$T^* = 1 - \varphi \tag{9}$$

The difference in metal temperature between uncoated and ceramic-coated vanes can be found from

$$\Delta T_w = T_c + \Delta T^* (T_g - T_c) \tag{10}$$

where

$$\Delta T^* = T^*_{uc} - T^*_{TBC}$$

RESULTS AND DISCUSSION

The experimental program was divided into four parts: tests on uncoated vanes, tests on vanes with two ceramic coating thicknesses, and tests on vanes with simulated coating loss. Data for the first three parts of the program covered a range of Reynolds numbers representing current and advanced gas turbines. The fourth part investigated coating loss at just one Reynolds number condition.

A radial crack developed in the ceramic coating near the leading edge of test vane 3 during the simulated-coating-loss tests. The crack apparently propagated along the edge of a thermocouple slot and is thought to be caused either by high stress concentrations or by the relative movement between the thermocouple cover material and the airfoil during thermal cycling, or by a combination of both effects.

Uncoated Vane

The data presented in this report were taken over a range of gas inlet Reynolds numbers from about 0.28×10^5 to 1.65×10^5. Typical dimensionless, chordwise temperature distributions for the uncoated vane, representing significant features within this Reynolds number range, are shown in figure 6. Uncorrected experimental data only are shown. The apparent laminar boundary layer on the vane suction surface at a low inlet Reynolds number (curve A) and the apparent turbulent boundary layer at high inlet Reynolds numbers (curve C), for similar coolant- to gas-flow ratios, show that the results are sensitive to the gas conditions. The gas conditions, represented by curves D and E, apparently result in a transitional boundary layer on the vane suction surface at these intermediate Reynolds numbers. The nature of the boundary layer could not be determined precisely; however, these conclusions can be deduced from the shape of the wall temperature profiles of curves A and C. These profiles are of the same form as that predicted by assuming a laminar or turbulent heat-transfer-coefficient distribution, respectively. Consequently, as the gas conditions were changed, increasing the inlet Reynolds number from 0.6×10^5 to 1.65×10^5, the vane suction-surface boundary layer changed from laminar through a transitional regime to a turbulent state. For the purposes of this report the boundary layer is referred to as laminar or turbulent. The boundary-layer status on the pressure surface did not appear to change over the Reynolds number range investigated. That is, the shape of the vane metal temperature profile was not affected by increasing the Reynolds number.

Thermal-Barrier-Coated Vane

High Reynolds number. - The effectiveness of the ceramic coating in reducing airfoil metal temperatures is shown by the chordwise dimensionless temperature distributions in figure 7(a). These distributions (for an uncoated vane and for a vane with two ceramic coating thicknesses) represent data taken at similar gas conditions and nearly equal coolant- to gas-flow ratios (~0.052). These data are for a high inlet gas Reynolds number, where a fully turbulent gas boundary layer exists on both surfaces of the ceramic coated and uncoated vanes.

Also shown in the figure are corrected distributions where, to simplify the calculation procedure, the correction factor is based on overall average gas conditions and not on local gas conditions. As long as the local gas-side heat-transfer coefficient does not vary substantially from the average, this approach does not significantly affect the results. However, if laminar and turbulent boundary layers are present, local conditions must be considered. It is interesting that the correction for the uncoated-vane temperatures results in higher wall-temperature levels at engine conditions than would other-

wise be predicted from uncorrected test data. When a ceramic coating is applied to the vane, the temperature correction results in lower wall-temperature levels at engine conditions.

The 0.025-centimeter- (0.01-in.-) thick coating reduced the metal temperature substantially on both the suction and pressure surfaces, as indicated in figure 7. This reduction, at test conditions, was nominally about 26 and 41 kelvins (47 and 74 deg F), respectively. When scaled to engine conditions and corrected, the predicted metal-temperature reductions become 120 and 135 kelvins (216 and 243 deg F), respectively, for the 0.025-centimeter- (0.01-in.-) thick coating and 215 and 235 kelvins (387 and 423 deg F), respectively, for the 0.050-centimeter- (0.02-in.-) thick coating. Along with the reduction in metal-temperature level, there was also a reduction in the temperature gradient in the leading-edge region.

Because the ceramic coating was feathered out to a negligible thickness near the trailing edge of the pressure surface, the last thermocouple location should indicate approximately the same temperature level for all three test points. This is the case as observed in figure 7(a).

Low Reynolds number. - Adding a ceramic coating to a turbine vane can influence the development of the boundary layer because of the increased surface roughness, increased external dimensions (reduced channel dimensions), and the potentially wavy surface contour after coating. Particularly sensitive to changes in the vane surface condition is the boundary-layer transition location. Figure 7(b) shows the effects of adding a 0.025-centimeter- (0.01-in.-) thick coating to a turbine vane operating at a low gas inlet Reynolds number of 0.28×10^5 and a coolant- to gas-flow ratio of about 0.045. The coating apparently tripped the boundary layer on the suction surface and led to an increased heat flux to the vane. This resulted in higher metal wall temperatures rather than lower temperatures. The ceramic-coated surface was polished to a finish of about 3 micrometers rms (120 μin.), as discussed in the section Thermal-Barrier Coating. This compares to metal surface finishes of about 1 micrometer rms (40 μin.). The ceramic coating reduced the wall temperature on the pressure surface as expected.

Average cooling effectiveness. - The average vane cooling effectiveness (corrected and uncorrected) at a high inlet gas Reynolds number is shown in figure 8 as a function of the coolant- to gas-flow ratio for the uncoated vane and for the vane with two ceramic coating thicknesses. The average vane temperature used is based on an area-weighted average of the measured midspan vane temperatures.

The average cooling efficiency increases as the coating thickness increases. This implies a decrease in metal wall temperature with an increase in coating thickness. The average temperature reductions attainable, when the data are properly scaled and corrected, are 122 K (220° F) for the 0.025-centimeter- (0.01-in.-) thick coating and 212 K (382° F) for the 0.050-centimeter- (0.02-in.-) thick coating. The average cooling

efficiency results are similar to the results depicted in figure 7(a) for local ceramic coating benefits.

Effect of Coating Loss

The effects of coating spallation on the metal wall temperature are shown in figure 9. This condition was simulated by removing a portion of the coating in the leading- and trailing-edge regions. Dimensionless chordwise temperature distributions are shown in figure 9 for the uncoated vane, the vane with a 0.050-centimeter-thick coating, and the vane with segments of the 0.050-centimeter-thick coating removed.

Figure 9(a) shows these temperature distributions for vane 3, which had a simulated coating loss on the pressure surface near the leading edge. The data are for engine conditions with a relatively low gas inlet Reynolds number. The results indicate that, even though wall temperature sharply increased at the damaged area, the level remained below that of the uncoated vane. This is attributed to heat conduction to the cooler metal surrounding the damaged area. In addition, the overall temperature increase was limited to the leading-edge portion of the vane although the coating had probably cracked and loosened around the leading edge during the test (fig. 4).

Figure 9(b) shows the result of simulated coating loss at two locations on the suction surface of vane 2. The wall temperature sharply increased at the point of damage near the leading edge, and the effects persisted over 70 percent of the suction surface and extended to the simulated coating loss near the trailing edge. In the leading-edge region, the wall temperature of the coated vane always remained below that of the uncoated vane. This was not true at the damage location on the trailing edge. The uncoated vane apparently had a laminar boundary layer on the suction surface, as discussed in the section Uncoated Vane, that was tripped to a turbulent condition by the ceramic coating and resulted in a substantial increase in heat flux to the suction surface. This, in turn, led to the higher temperature at the point of damage.

The reason for the metal-temperature increase along the entire suction surface downstream of the damaged area can be deduced from figure 10. This figure is a photograph taken with a conventional camera and infrared-sensitive film. The detected radiation from the vane surface was restricted to a narrow wavelength interval of 0.85 to 0.90 micrometer by a combination of the IR film and a filter. This wavelength interval was selected because the intervening hot gas was transparent in this region. The halo at the edge of the ceramic coating surrounding the damaged area and the lighter shading of the ceramic surface downstream resulted from the higher surface temperatures in this region. The darker areas in the photograph indicate lower temperatures relative to the lighter regions. The surface roughness or boundary-layer trip created

by the surface discontinuity at the coating damage location increased the turbulence and friction in the gas stream and apparently resulted in early transition or boundary-layer separation in a localized region.

SUMMARY OF RESULTS

This report presents the results of an experimental investigation into how a ceramic thermal-barrier coating affects the metal temperatures of an air-cooled turbine vane. The effects of coating loss were also examined. Data were taken at test conditions simulating typical gas-turbine engines at both takeoff and cruise operation. A correction factor was applied to the test data to correct for material thermal conductivity differences between engine conditions and similarity-derived test conditions. The following results were obtained:

1. The ceramic thermal-barrier coating significantly improved the cooling effectiveness of the turbine vane at high inlet gas Reynolds number conditions (turbulent flow). The airfoil metal temperatures decreased as the ceramic coating thickness increased. The average airfoil metal-temperature reductions at engine conditions are predicted to be 122 and 212 kelvins (220 and 382 deg F) for ceramic coating thicknesses of 0.025 and 0.050 centimeter (0.010 and 0.020 in.), respectively.

2. The local chordwise metal-temperature gradients were also reduced at high inlet gas Reynolds number conditions by application of the ceramic coating.

3. At low inlet gas Reynolds number conditions (laminar flow), airfoil metal temperatures on the suction surface of the ceramic-coated vane were equal to or greater than those of the uncoated turbine vane. The changed surface condition of the coated vane, despite a polishing procedure to smooth the coating surface, was apparently sufficient to trip the laminar boundary layer and increase the heat flux to the vane.

4. The ceramic coating, with local coating loss in the leading-edge region, still provided some thermal protection for the vanes even though temperature spikes were observed at the point of coating loss. The local and average metal temperatures were generally lower than those observed without the thermal-barrier coating. The exception was the trailing edge, where the metal temperature was higher with the coating loss than without any coating. This was the result of tripping a laminar boundary layer to the turbulent state.

Lewis Research Center,
National Aeronautics and Space Administration,
Cleveland, Ohio, September 14, 1979,
505-04.

REFERENCES

1. Liebert, Curt H.; and Stepka, F. S.: Potential Use of Ceramic Coating as a Thermal Insulation on Cooled Turbine Hardware. NASA TM X-3352, 1976.

2. Colladay, R. S.: Importance of Combining Convection with Film Cooling. AIAA Paper 72-8, Jan. 1972.

3. Moffitt, Thomas P.; Stepka, F. S.; and Rohlik, H. E.: Summary of NASA Aerodynamic and Heat Transfer Studies in Turbine Vanes and Blades. SAE Paper 760917, Nov. 1976.

4. Liebert, C. H.; and Stepka, F. S.: Ceramic Thermal-Barrier Coatings for Cooled Turbines. AIAA Paper 76-729, July 1976.

5. Liebert, C. H.; et al.: Durability of Zirconia Thermal-Barrier Ceramic Coatings on Air-Cooled Turbine Blades in Cyclic Jet Engine Operation. NASA TM X-3410, 1976.

6. Stecura, Stephan; and Liebert, Curt H.: Thermal Barrier Coating System. U.S. Patent 4,055,705, Oct. 1977.

7. Stepka, Francis S.; Liebert, Curt H.; and Stecura, Stephan: Summary of NASA Research on Thermal-Barrier Coatings. SAE Paper 770343, 1977.

8. Calvert, Howard F.; et al.: Turbine Cooling Research Facility. NASA TM X-1927, 1970.

9. Gladden, Herbert J.; et al.: Aerodynamic Investigation of Four-Vane Cascade Designed for Turbine Cooling Studies. NASA TM X-1954, 1970.

10. Crowl, Robert J.; and Gladden, Herbert J.: Methods and Procedures for Evaluating, Forming, and Installing Small-Diameter Sheathed Thermocouple Wire and Sheathed Thermocouples. NASA TM X-2377, 1971.

11. Sucec, James: Application of Differential Similarity to Finding Nondimensional Groups Important in Tests of Cooled Engine Components. NASA TM X-3484, 1977.

12. Gladden, Herbert J.; and Livingood, John N. B.: Procedure for Scaling of Experimental Vane Airfoil Temperatures from Low to High Gas Temperatures. NASA TN D-6510, 1971.

13. Colladay, Raymond S.; and Stepka, Francis S.: Similarity Constraints in Testing of Cooled Engines Parts. NASA TN D-7707, 1974.

14. Gladden, Herbert J.: Extension of Similarity Test Procedures to Cooled Engine Components with Insulating Ceramic Coatings. NASA TP-1615, 1980.

15. Poferl, David J.; Svehla, Robert A.; and Lewandowski, Kenneth: Thermodynamic and Transport Properties of Air and the Combustion Products of Natural Gas and of ASTM-A-1 Fuel with Air. NASA TN D-5452, 1969.

16. MAR-M 302. High Temperature Strength Nickel Base Alloys, The International Nickel Co., Inc., Rev. ed., 1964, Table III, p. 9.

17. Liebert, Curt H.; and Stepka, Francis S.: Industry Tests of NASA Ceramic Thermal Barrier Coating. NASA TP-1425, 1979.

TABLE I. - THERMOCOUPLE LOCATIONS AND COATING THICKNESS

Thermocouple	Distance from leading edge, cm	Dimensionless distance	Test part 2	Test part 3
			Ceramic coating thickness[a], cm	
Suction surface; L = 7.42 cm				
1	6.42	0.866	0.033,0.028	0.043,0.053
2	5.07	.684	0.030,0.028	0.033,0.058
3	3.88	.523	0.028,0.028	0.051,0.061
4	2.60	.351	0.041,0.041	0.048,0.033
5	1.32	.178	0.030,0.030	0.058,0.023
6	.50	.067	0.023,0.041	0.053,0.043
7	0	0	0.025,0.028	0.084,0.084
Pressure surface; L = 6.45 cm				
8	0.39	0.061	0.013,0.028	0.084,0.091
9	1.25	.194	0.023,0.020	0.051,0.084
10	2.52	.391	0.018,0.020	0.053,0.076
11	3.78	.586	0.015,0.020	0.048,0.058
12	4.85	.752	----------	----------

[a]First value is for vane 2; second value is for vane 3. Tolerance, ±0.002 cm.

TABLE II. - COMPARISON OF TEST AND ENGINE CONDITIONS

Case	Cascade test conditions			Engine similarity conditions			Gas inlet Reynolds number	Aircraft type (and flight condition)
	Gas temperature, K	Gas pressure, N/cm^2	Coolant temperature, K	Gas temperature, K	Gas pressure, N/cm^2	Coolant temperature, K		
A	890	44.8	290	1770	97.2	590	0.597×10^5	SST (takeoff)
B	1260	32.4	570	1770	47.6	810	.284	SST (cruise)
C	590	75.2	300	1590	243	760	1.647	CTOL (takeoff)
D	930	53.1	430	1590	102.3	730	.713	CTOL (cruise)
E	930	64.1	450	1590	123.6	770	.865	VTOL (cruise)
F	1530	86.2	290	1530	86.2	680	.500	STOL (cruise)

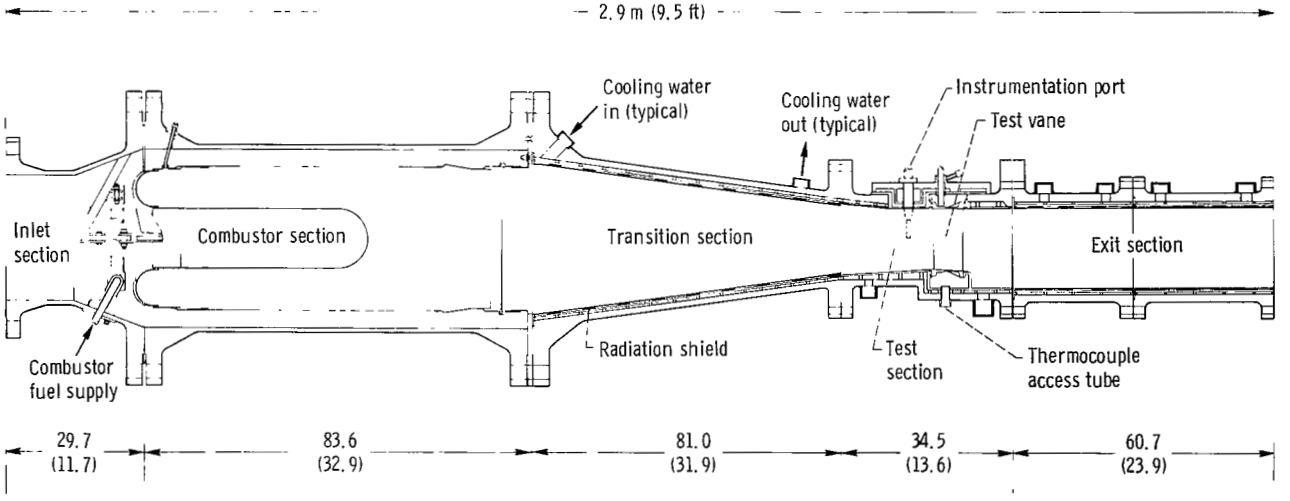

(a) Cross-sectional view of main components. (Dimensions are in cm (in.) unless noted.)

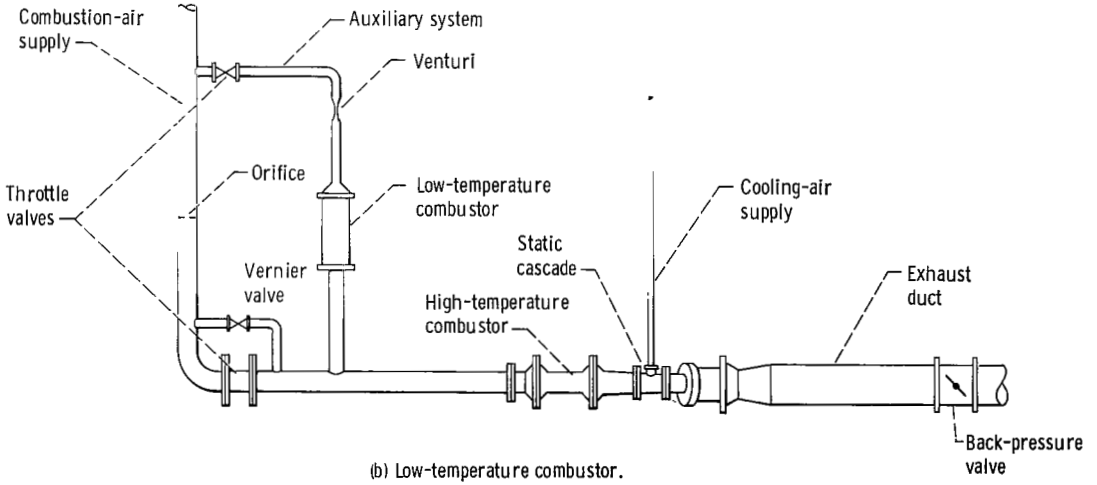

(b) Low-temperature combustor.

Figure 1. - Cascade facility.

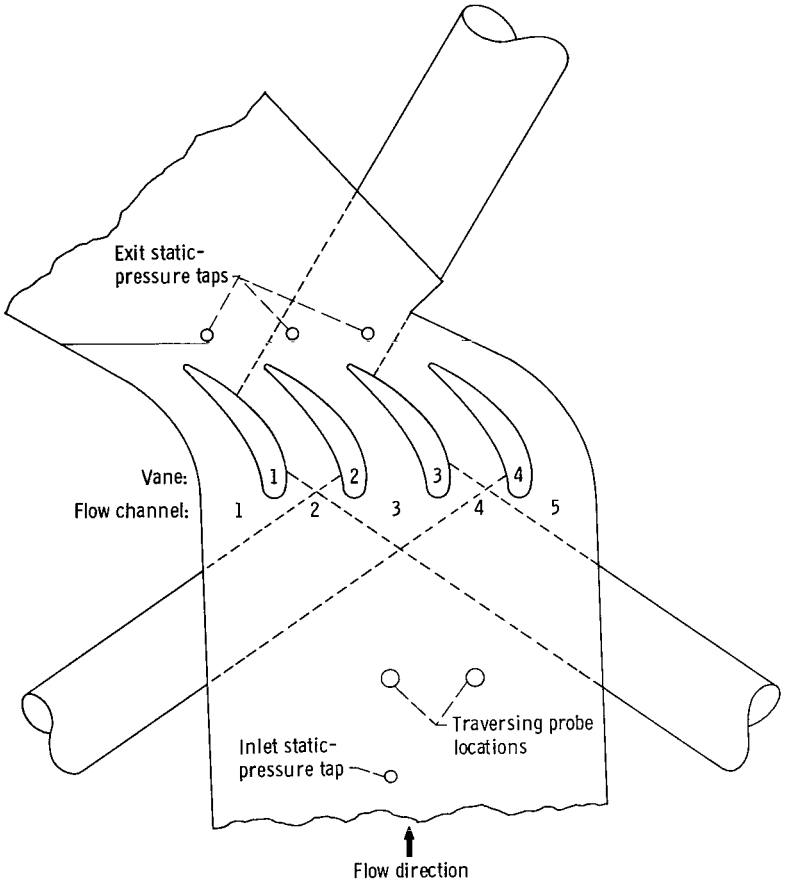

Figure 2. - Vane row and location of instrumentation stations in static cascade test section.

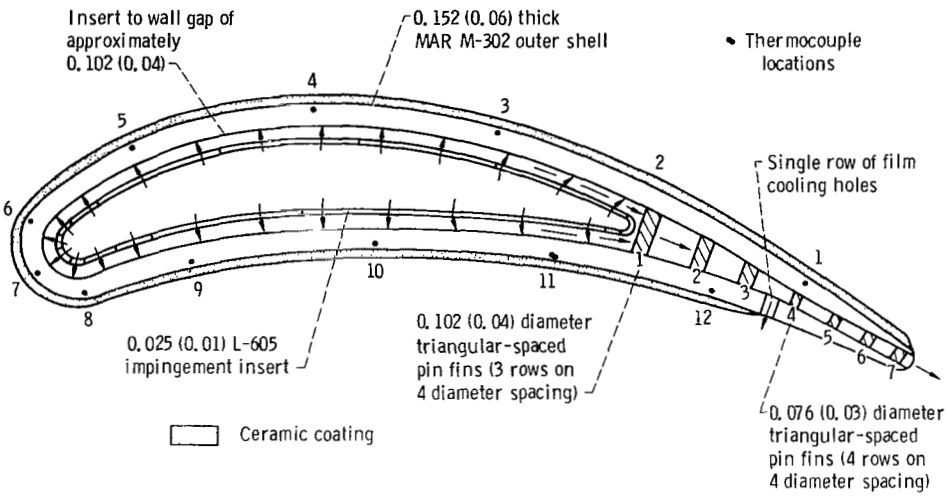

(a) Cross-sectional midspan view of test vane, showing the internal cooling configuration and the thermocouple locations. (Dimensions are in cm (in.) unless otherwise noted.)

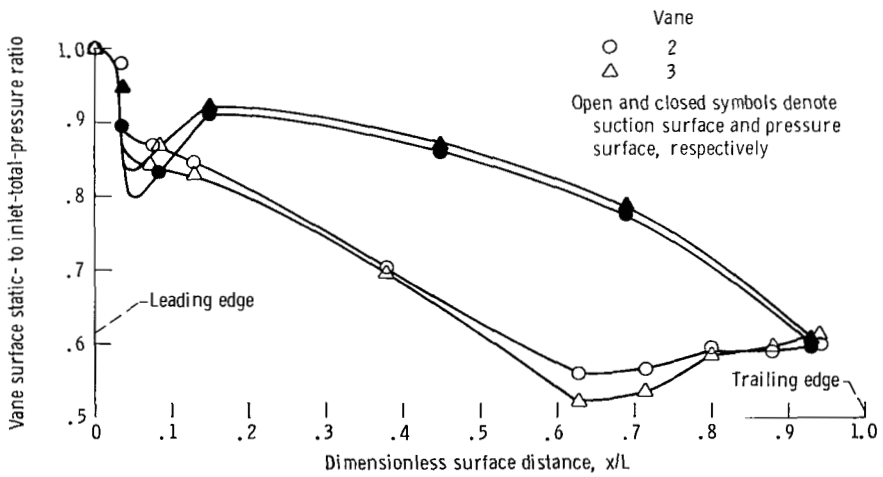

(b) Experimental static- to inlet-total-pressure ratio distribution of a solid vane in cascade facility.

Figure 3. - Turbine vane configuration investigated.

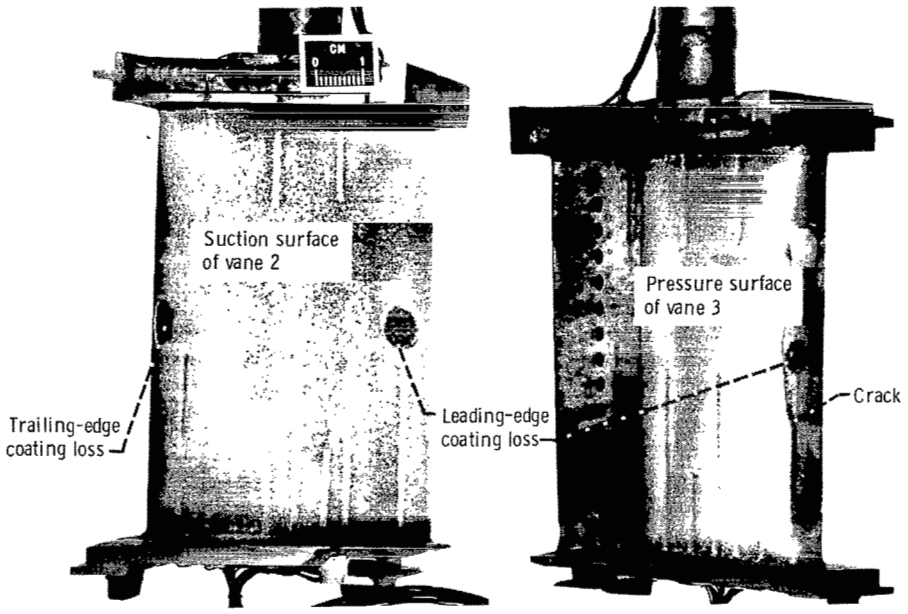

Figure 4. - Ceramic-coated test vanes showing simulated coating loss. (Note crack in coating at leading edge of vane 3.)

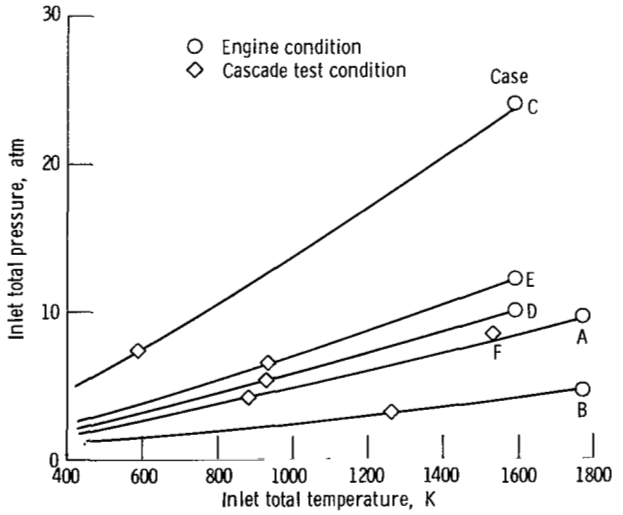

Figure 5. - Similarity curves of constant-momentum-thickness Reynolds number and critical Mach number, showing both engine and cascade test conditions.

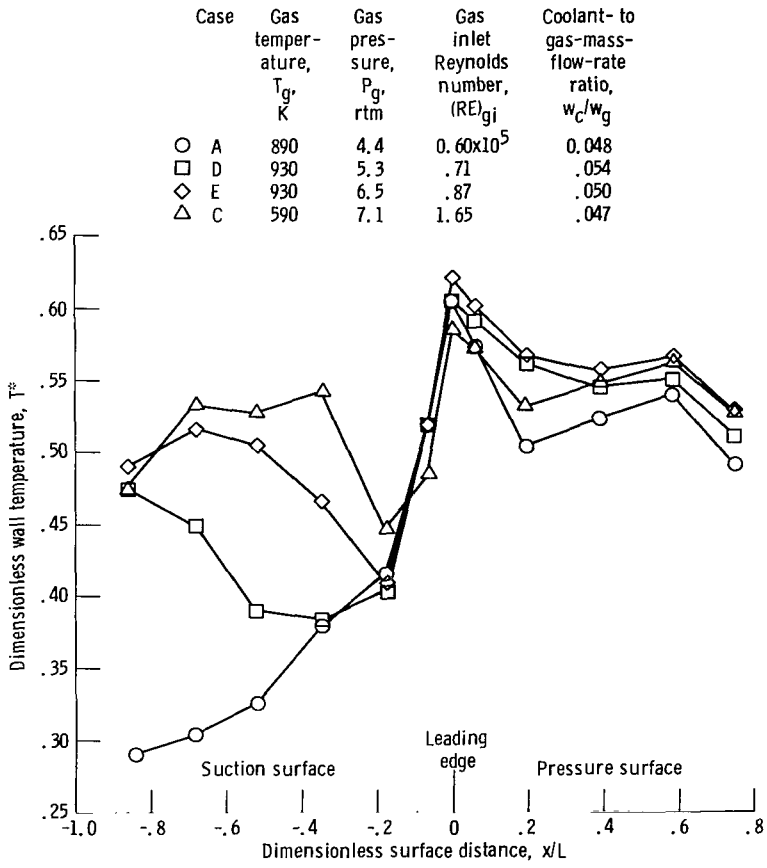

Figure 6. - Dimensionless wall-temperature distributions showing effect of inlet Reynolds number (uncoated turbine vane).

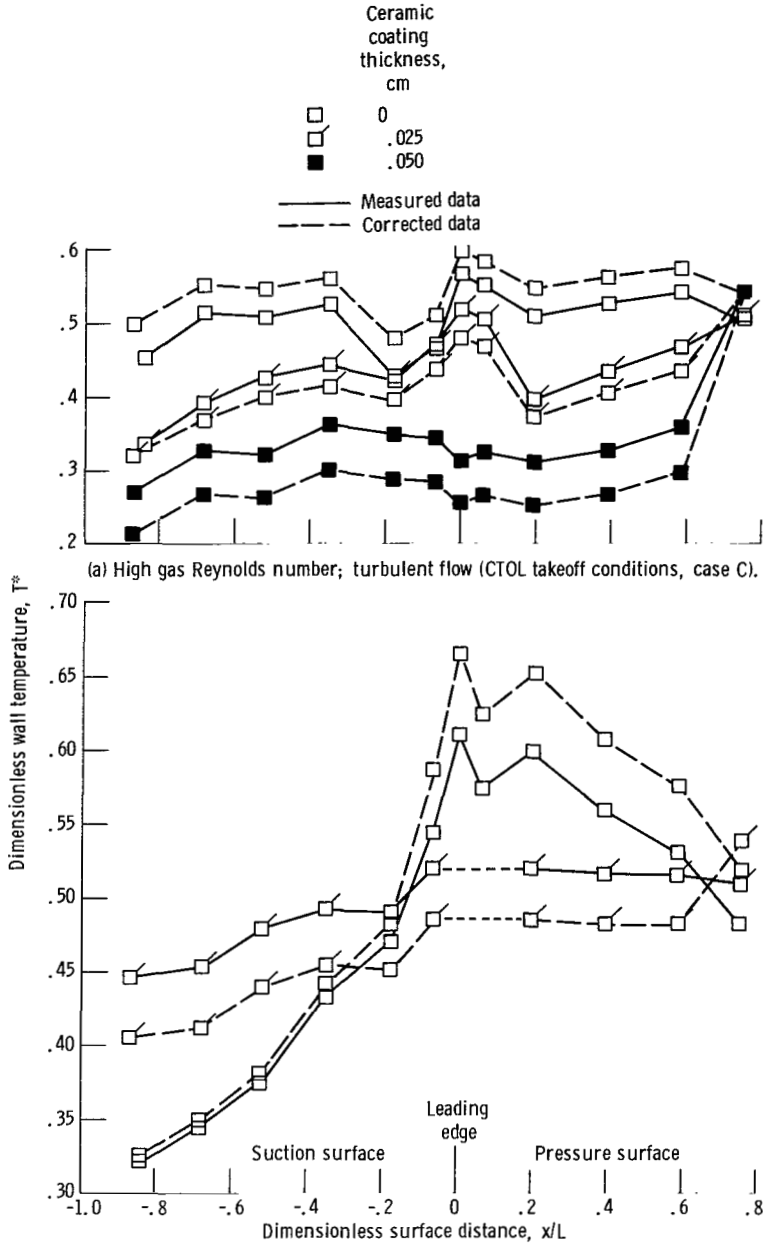

(a) High gas Reynolds number; turbulent flow (CTOL takeoff conditions, case C).

(b) Transition of laminar boundary layer on suction surface with addition of ceramic coating (SST cruise conditions, case B).

Figure 7. - Dimensionless wall-temperature distributions for a ceramic coated and an uncoated vane.

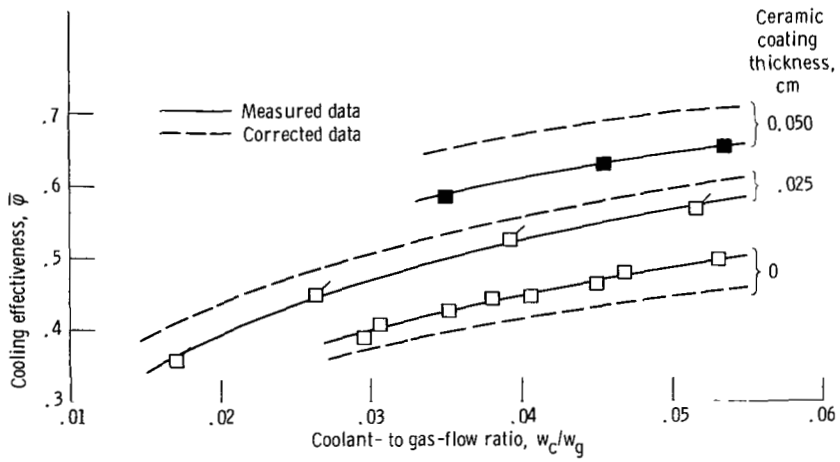

Figure 8. - Average cooling effectiveness of an uncoated vane and a vane with two ceramic coating thicknesses (CTOL takeoff conditions, case C).

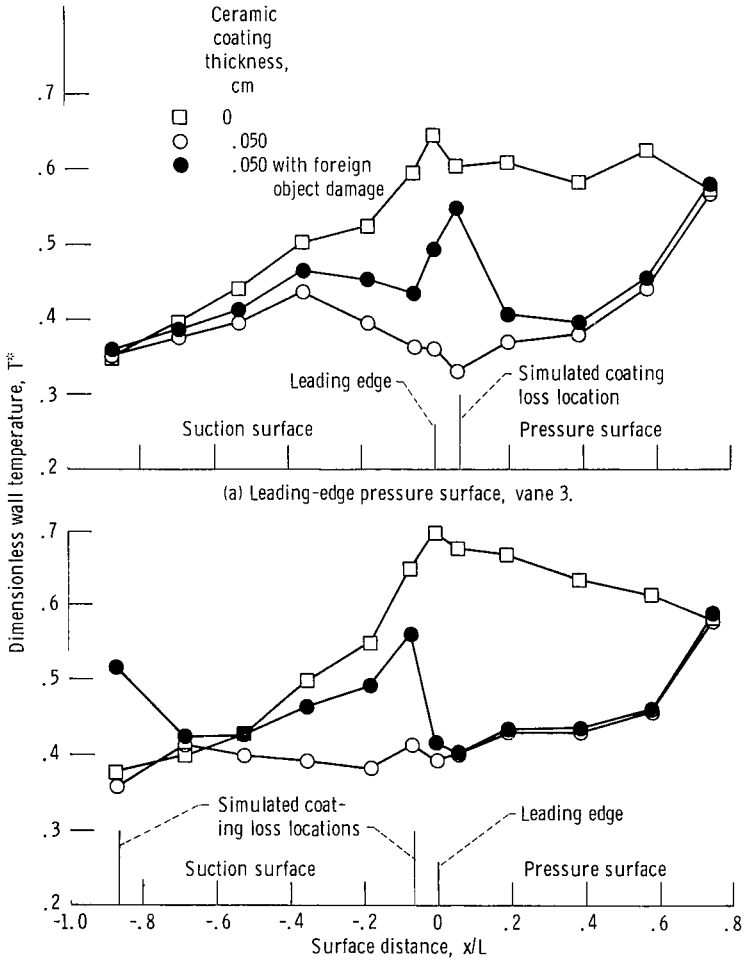

(a) Leading-edge pressure surface, vane 3.

(b) Leading- and trailing-edge suction surface, vane 2.

Figure 9. - Dimensionless temperature distributions showing effects of simulated coating loss (STOL cruise conditions, case F).

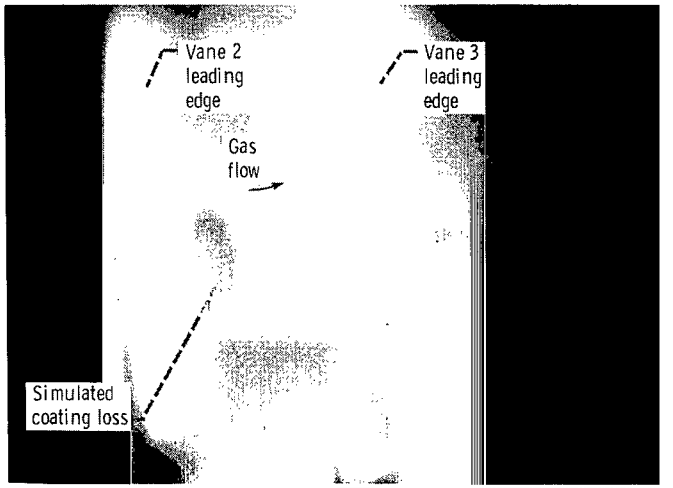

Figure 10. - Infrared photograph of leading-edge suction surface, showing simulated coating loss.

1. Report No.	2. Government Accession No.	3. Recipient's Catalog No.
NASA TP-1598		

4. Title and Subtitle	5. Report Date
EFFECTS OF A CERAMIC COATING ON METAL TEMPERATURES OF AN AIR-COOLED TURBINE VANE	February 1980
	6. Performing Organization Code

7. Author(s)	8. Performing Organization Report No.
Herbert J. Gladden and Curt H. Liebert	E-167
	10. Work Unit No. 505-04

9. Performing Organization Name and Address	11. Contract or Grant No.
National Aeronautics and Space Administration Lewis Research Center Cleveland, Ohio 44135	
	13. Type of Report and Period Covered
12. Sponsoring Agency Name and Address	Technical Paper
National Aeronautics and Space Administration Washington, D.C. 20546	14. Sponsoring Agency Code

15. Supplementary Notes

16. Abstract

The metal temperatures of an air-cooled turbine vane both uncoated and coated with the NASA thermal-barrier system were studied experimentally. Current and advanced gas-turbine-engine conditions were simulated but at reduced temperatures and pressures. Airfoil metal temperatures were significantly reduced, both locally and on the average, by use of the coating. However, at low gas Reynolds number, the ceramic coating tripped a laminar boundary layer on the suction surface, and the resulting higher heat flux increased the metal temperatures. Simulated coating loss was also investigated and was shown to increase local metal temperatures. However, the metal temperatures in the leading-edge region remained below those of the uncoated vane tested at similar conditions. Metal temperatures in the trailing-edge region exceeded those of the uncoated vane.

17. Key Words (Suggested by Author(s))	18. Distribution Statement
Heat transfer Turbine cooling Thermal barrier coating Coating spallation	Unclassified - unlimited STAR Category 34

19. Security Classif. (of this report)	20. Security Classif. (of this page)	21. No. of Pages	22. Price*
Unclassified	Unclassified	28	A03

* For sale by the National Technical Information Service, Springfield, Virginia 22161

NASA-Langley, 1980

National Aeronautics and
Space Administration

Washington, D.C.
20546

THIRD-CLASS BULK RATE

Postage and Fees Paid
National Aeronautics and
Space Administration
NASA-451

Official Business
Penalty

1 1 1U,D, 122179 S00903DS
DEPT OF THE AIR FORCE
AF WEAPONS LABORATORY
ATTN: TECHNICAL LIBRARY (SUL)
KIRTLAND AFB NM 87117

NASA

POSTMASTER: If Undeliverable (Section 158 Postal Manual) Do Not Return